ACS OMEGA

Open Access

http://pubs.acs.org/journal/acsodf

Article

Enhanced Stability and Sensitivity for CA-125 Detection Under Microfluidic Shear Flow Using Polyethylene Glycol-Coated Biosensor

Yudong Wang, Niladri Talukder, Bharath Babu Nunna, Ming Lu, Xiao Tong, and Eon Soo Lee*

Cite This: *ACS Omega* 2025, 10, 692−702

Read Online

ACCESS | Metrics & More | Article Recommendations | Supporting Information

ABSTRACT: The microfluidic-based point-of-care (POC) diagnostic tool has garnered significant interest in recent years, offering rapid and cost-effective disease detection. There is a growing trend toward integrating microfluidic platforms with biosensors, aligning lab-on-a-chip technologies with POC diagnostic devices. Despite numerous efforts to incorporate biosensors into microfluidic systems, researchers have performed very limited investigations on the stability of biomarker detection when biosensors operate under microfluidic shear flow conditions. Gold nanoparticles (AuNPs) are a widely employed material in capacitive biosensors for antibody immobilization and sensitivity enhancement. However, AuNPs have limitations in providing stable detection of biomarkers within microfluidic shear flow due to their agglomeration nature. This study addresses these limitations by employing 2 kDa polyethylene glycol (PEG) as an intermediate biofunctional layer to immobilize CA-125 antibodies on gold-interdigitated electrodes for the stable and accurate detection of CA-125 antigens. The stabilities and sensitivities of AuNPs and PEG-coated biosensors are evaluated under both static drop and microfluidic shear flow conditions for CA-125 antigen detection. The experimental results demonstrate a capacitive signal response (5660 pF at 10 kHz) 2.2 times higher using the PEG-coated biosensor than the signal (2551 pF at 10 kHz) measured by the AuNP-coated biosensor in the detection of CA-125 antigen−antibody conjugation under static drop conditions, indicating the higher sensitivity of the PEG-coated biosensor. Additionally, the PEG-coated biosensor exhibits better consistency for the CA-125 antigen detection between static drop and microfluidic shear flow conditions (Cp decrease in percentage ($\Delta Cp\%\downarrow$) = 2.9% at 10 kHz) compared to the electrical signals measured using the AuNP-coated biosensor ($\Delta Cp\%\downarrow$ = 32.4% at 10 kHz), which suggests that the PEG-coated biosensor demonstrates higher stability for CA-125 antigen detection under microfluidic shear flow conditions. With these significant improvements brought by the PEG-coated biosensor, especially under microfluidic conditions, a substantial hurdle in developing electrical biosensors for POC diagnostic applications has been overcome, expediting further advancements in the field.

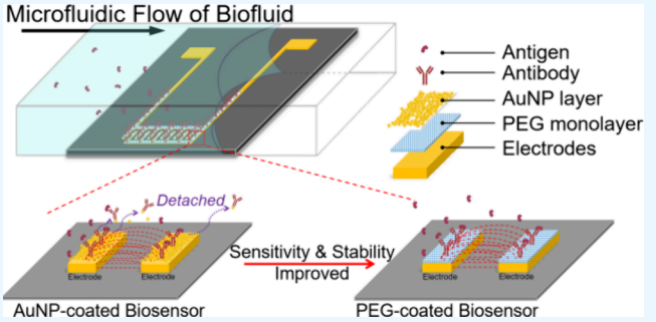

1. INTRODUCTION

Label-free affinity biosensor-based diagnoses have attracted numerous investigations as an alternative method to the enzyme-linked immunosorbent assay (ELISA) due to the features of low-cost and real-time detection of the analytes.[1] Researchers have developed various biosensors based on the different transducer types: optical biosensors,[2] electrochemical biosensors,[3] piezoelectric biosensors,[4] thermometric biosensors,[5] etc. Among the various types of label-free biosensors, electrochemical biosensors have garnered particular attention due to their suitability for point-of-care (POC) devices.[6] These sensors convert biomolecular reactions into changes in electrical signals, such as current, voltage, impedance, and capacitance.[7] Specifically, capacitive biosensors measure changes in dielectric properties and the thickness of dielectric layers at the interface between the biosolution and the biosensor surface.[8] These biosensors offer advantages such as miniaturization, standalone operation, real-time results, and low power consumption, making them ideal for POC applications.[9]

Since the electrical biosensor was first integrated into the microfluidic platform in 2005 and reported by Bange et al.,[10] the applications of electrical biosensors in POC devices have been expanded rapidly due to the portability provided by microfluidic platforms. Integrating the biosensor into a microfluidic platform significantly simplifies the sample preparation process in the assays. This integration reduces the required sample volume from milliliters (mL) to microliters (μL) and streamlines sample treatments, such as

Received: August 16, 2024
Revised: October 31, 2024
Accepted: November 5, 2024
Published: December 20, 2024

cell concentration and filtration. As a result, microfluidic-based biosensors hold great potential for expansion as point-of-care (POC) diagnostic devices.[11−17] Although much research has been reported on microfluidic-based biosensing systems for disease diagnoses, most of those systems relied on external pumping systems or other flow control devices to process and deliver the analytes to the biosensors.[18−22] In this study, the flow in the microchannel is self-driven due to capillary action activated by the meticulous modification of the hydrophilicity on the microchannel surface.[23]

Mucin-16, also known as ovarian cancer-related tumor marker CA-125, is a widely used biomarker for the detection and monitoring of ovarian cancer.[24] Ovarian cancer is known as a silent killer because it has no specific symptoms in the early stage. Additionally, the 5 year survival rates of ovarian cancer patients are varied from 93% at an early stage to 30% at an advanced stage. As such, early detection of CA-125 using a POC device can significantly encourage potential patients to take early screening for ovarian cancer and increase their survival chance.[25,26] CA-125 is a unique protein with a large molecular weight (110 kDa to 2000 kDa) due to high variable glycosylation, making the detection of it critical in biosensing research.[27]

Many researchers have reported studies on CA-125 detection using electrical biosensors in microfluidic platforms.[28−32] The performance of microfluidic capacitive biosensors is typically dependent on several primary factors, such as probe immobilization, the specific binding between the antigen and antibody, and the dielectric properties of the immobilized probe.[33] Daniels et al. noted that probe immobilization technology can enhance microfluidic immunoassay biosensors.[34] Various probe immobilization techniques with different types of biocompatible nanomaterials, such as carbon nanotubes (CNTs),[35,36] porous carbon nanofibers,[37] gold nanoparticles (AuNPs),[38−45] and other nanomaterials of noble metals like silver, palladium, rhodium, platinum, etc., have been reported recently.[46] Ravalli et al. reported using AuNPs coated on a screen-printed graphite electrode to detect the CA-125 antigen in a PBS solution but not in a microfluidic condition.[40] Nunna et al. used AuNPs coated on interdigitated gold electrodes to immobilize the CA-125 antibody and successfully detected the CA-125 antigen in a microfluidic condition with enhanced sensitivity.[35] However, fluid flow in the microchannel induces a shear effect on the biosensor's surface, which can negatively impact biosensing stability by causing immobilized probes to detach.[47] Several studies have attempted to address the issue of probe immobilization stability for DNA and protein binding within microfluidic platforms.[48,49] To the best of the author's knowledge, no reported technique has successfully enhanced the stability of antigen detection in capacitive biosensors under microfluidic shear flow conditions. The lack of stability in the microfluidic flow conditions will decrease the signal-to-noise ratio and make the detection results unreliable. This challenge hinders the development of microfluidic capacitive immunobiosensors and needs to be addressed without compromising the antigen detection performance.

In this study, we utilized functionalized poly(ethylene glycol) "thiol-PEG-carboxyl (HS-PEG2000-COOH)" as the biofunctional layer to immobilize the CA-125 antibody onto the surface of interdigitated gold electrodes, which function as the capacitive biosensor for CA-125 antigen detection. Polyethylene glycol (PEG) is a polymer material of increasing significance in biosensing technology due to its nonfouling, nonimmunogenic, nonantigenic, and hygroscopic properties, making it an excellent candidate for probe immobilization on the biosensor.[50] The PEG with 2 kDa molecular weight provides a smooth monolayer onto the biosensor surface through the covalent bond and mitigates the shear flow effect on the immobilized antibodies. Additionally, its hydrophilic and hygroscopic properties contribute to PEG's substantial potential in microfluidic biosensing systems by providing a stable and polar aqueous sensing environment.[51]

This paper presents a study of CA-125 antigen detection with enhanced sensing stability and sensitivity using a PEG-coated biosensor under microfluidic shear flow conditions. The sensing stability of this PEG-coated biosensor was compared to that of a biosensor coated with AuNP, which is one of the most used materials in biosensors. Furthermore, we investigated the sensitivity of antigen−antibody conjugation using the capacitive biosensor coated with PEG, comparing it to the sensitivity of the AuNP-coated biosensor. This comparison provides experimental evidence of the advantages of PEG in a microfluidic sensing environment. The minimal variation in the sensing signal observed under both microfluidic shear flow and static drop conditions highlights a promising technique for the development of microfluidic capacitive biosensors. Meanwhile, PEG's lower cost and ease of fabrication perfectly fit the point-of-care diagnostic device applications and have a higher potential for commercialization.

2. METHODS AND EXPERIMENTS

2.1. Chemicals and Reagents. The 10 nm carboxylic functionalized (lipoic acid) gold nanospheres were purchased from NanoComposix. The thiol and carboxylic functionalized poly(ethylene) glycol (HS-PEG2000-COOH) was procured from Biopharma PEG. The thiourea (CH_4N_2S), phosphate buffer saline (PBS), 1-ethyl-3-(3-(dimethylamino)propyl) carbodiimide (EDC), and *N*-hydroxysuccinimide (NHS) were purchased from Millipore Sigma. The CA-125 monoclonal antibodies and CA-125 antigens were purchased from Medix Biochemica (USA). The polydimethylsiloxane (PDMS) base and curing agent were purchased from Ellsworth Adhesives. The 4 in. silicon wafer was purchased from Virginia Semiconductor, Inc. The reason for using this specific functionalized PEG is that the thiol group facilitates the formation of a PEG monolayer on the gold electrode surface, while the carboxyl group enables antibody immobilization via EDC/NHS coupling. The PEG2000 creates a brush-like, uniform coating that enhances antibody immobilization, improving the stability and performance of the biosensor compared to other molecular weights.[52]

2.2. Interdigitated Electrode Fabrication. The interdigitated electrodes were fabricated by using electron-beam lithography (EBL) technology. A Si wafer with an oxide layer was first cut into 0.5 × 1 square in. pieces as substrate. PMMA-A6, a positive photoresist, was then applied on top of the substrate and spin-coated for 5 s at 500 rpm, followed by 45 s at 3000 rpm, to form an approximately 300 nm thick PMMA layer. It was then irradiated by an electron beam using an EBL system (JEOL JBX6300-FS located in the Brookhaven National Laboratory) to structure the electrode patterns. Subsequently, the sample was developed in MIBK:IPA 3:1 solution for 120 s, rinsed in isopropyl alcohol (IPA) for 60 s, and then blow-dried with nitrogen. The electron-beam evaporator (Kurt J. Lesker PVD75) was employed to deposit

https://doi.org/10.1021/acsomega.4c07596
ACS Omega 2025, 10, 692−702

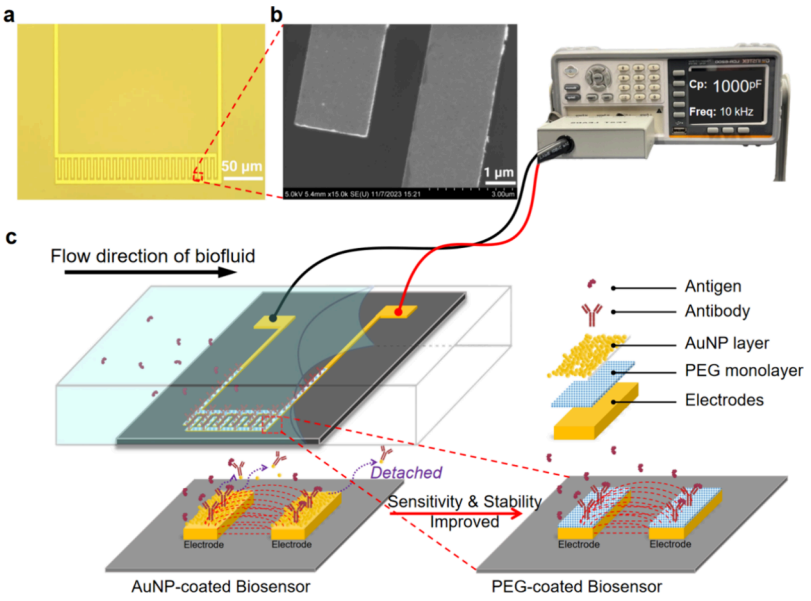

Figure 1. (a) Top view of the interdigitated gold electrodes with 200× magnification. (b) SEM image of gold interdigitated electrode surface. (c) Experimental setting of the PEG-coated biosensor for CA-125 antigen detection under the microfluidic flow condition and the comparison of AuNP and PEG-coated biosensors.

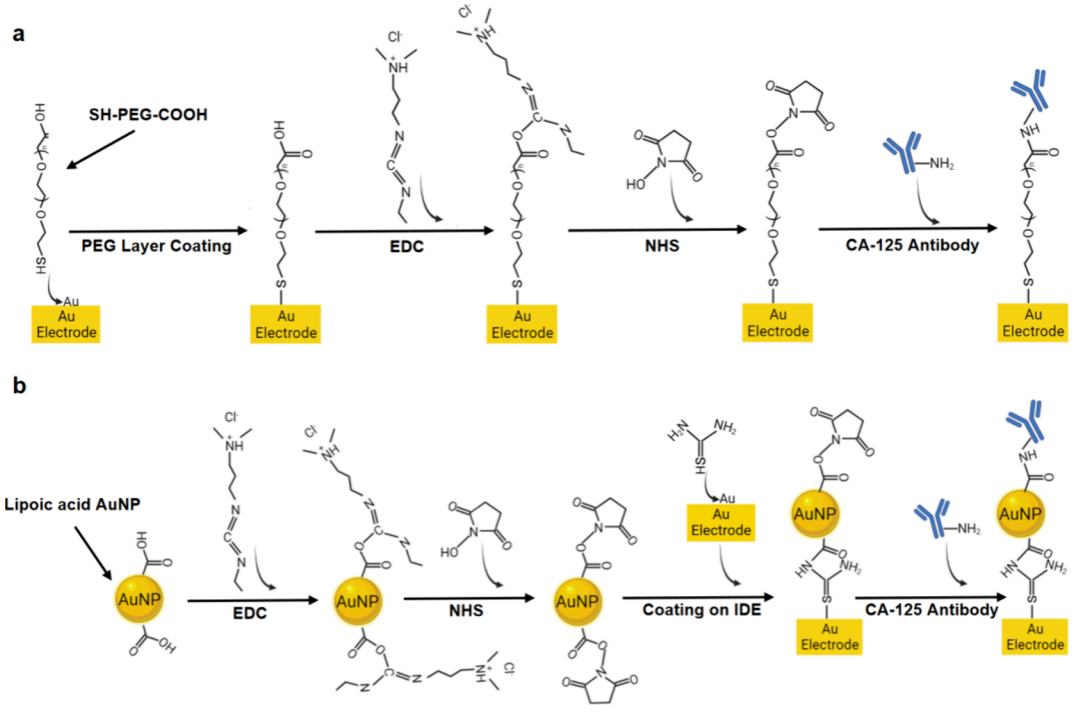

Figure 2. Schematic diagrams of (a) the coating and activation of the PEG layer and the immobilization of CA-125 antibodies on the PEG-coated biosensor and (b) the coating and activation of gold nanoparticles (AuNPs), the binding mechanisms between AuNPs and interdigitated electrodes (IDEs), and the immobilization of CA-125 antibodies on the AuNP-coated biosensor.

approximately 10 nm of chromium as an adhesion layer and then 90 nm of gold on top to reach the 100 nm target thickness of the interdigitated electrodes for the biosensing. Subsequently, a lift-off process using an acetone bath was conducted on the Si substrate to remove the unexposed PMMA resist. Following this step, the interdigitated gold electrodes were complete, as shown in Figure 1a,b, and the experimental settings are shown in Figure 1c. The fabrication process is demonstrated in Figure S1.

2.3. PEG-Coated Biosensor Fabrication. *2.3.1. PEG Layer Coating.* The interdigitated electrodes (IDEs) were thoroughly cleaned with acetone, IPA, and deionized (DI) water and dried with nitrogen stream to be ready for functional layers coating. The SH-PEG2000-COOH (2000 indicating the 2000 Da molecular weight) powder was dissolved into ethanol in a water bath at 50 °C to prepare the 7 mg/mL SH-PEG2000-COOH solution. The IDEs were immersed into the prepared PEG solution overnight (~16 h) during which the thiol group (−SH) of the SH-PEG-COOH thoroughly reacted

https://doi.org/10.1021/acsomega.4c07596
ACS Omega 2025, 10, 692−702

with the gold surface of the IDEs and formed the Au−S covalent bond to firmly form a monolayer of PEG on the IDE's surfaces, as shown in Figure 2a. The IDEs were rinsed with ethanol and DI water to remove the excess PEG and dried with a N_2 stream. The formation of the PEG layer was confirmed by the electrical signal reading from the electrical probe station (Signatone) and by the atomic force microscopy (AFM) image using Park NX-20 AFM, as discussed in Sections 3.1 and 3.3.1, respectively.

2.3.2. CA-125 Antibody Immobilization On the PEG Layer. The PEG-coated IDEs were activated (on the carboxylic acid group end of the PEG monolayer) with 100 mM EDC and 200 mM NHS. This process activated the carboxylic acid group of the PEG for antibody immobilization. After activation, the IDEs were rinsed with PBS to clean the surfaces and remove the residual solutions. Subsequently, the activated PEG-coated IDEs were incubated at 4 °C with 0.6 μL of 5 mg/mL CA-125 antibodies in PBS solution for 3 h to immobilize the CA-125 antibodies to the activated PEG layer using peptide bond. The biosensor (IDEs are defined as "biosensor" when the antibody is immobilized on the surface) was again rinsed with PBS to remove the nonimmobilized antibodies, and the nonreactive groups on the sensor were blocked using 1 M ethanolamine. After this, the sensor was rinsed with PBS and DI water and was ready for antigen detection. The surface activation and antibody immobilization are shown in Figure 2a.

2.4. AuNP-Coated Biosensor Fabrication. *2.4.1. Self-Assembled Monolayer (SAM) Coating.* The IDEs were immersed into the 50 mM thiourea solution in DI water overnight (∼12h). The Au−S covalent bond was formed by the reaction of the thiol group of thiourea and the gold surface of IDEs and the SAM layer was then coated on the IDEs, as shown in Figure 2b. The residual of thiourea was rinsed off using ethanol and DI water. The SAM can insulate the electrodes in the aqueous environment and bind with the gold nanoparticles for CA-125 antibody immobilization.

2.4.2. AuNP Coating. The AuNPs were activated with EDC and NHS, the same as PEG activation as described in Section 2.3.2. This process enables the lipoic acid gold particles (∼10 nm in diameter) to form peptide bonds with amine groups on the SAM layer and antibodies. The IDEs were coated with AuNPs by incubating them within the activated AuNPs solution for 2 h. Excess AuNPs were washed off with PBS and DI water.

2.4.3. CA-125 Antibody Immobilization on the AuNP. The AuNP-coated IDEs were incubated at 4 °C with 0.6 μL of 5 mg/mL CA-125 antibodies in PBS solution for 3 h to immobilize the CA-125 antibodies on the AuNPs by the peptide bond between the amine group and activated AuNPs. After incubation, the sensor surface was rinsed with PBS to remove the nonimmobilized antibodies, and the nonreactive groups on the sensor were blocked using ethanolamine. The sensor was rinsed with PBS and DI water, completing the fabrication of the AuNP-coated biosensor. The surface activation and antibody immobilization are shown in Figure 2b.

The comparison of the structures of the PEG-coated biosensor and AuNP-coated biosensor is shown in Figure S3 with step-by-step fabrication schematic diagrams.

2.5. Microchannel Fabrication. The microchannel was fabricated by using photolithography and soft lithography techniques. A 4 in. Si wafer was spin-coated with photoresist SU-8 2050 at 3300 rpm for 50 s to form a 60 μm-thick resist layer (same as the target microchannel height). After photoresist coating, the wafer was baked at 90 °C for 7 min. The microchannel patterns were exposed to the SU-8 coated wafer using a UV photolithography system (Karl Suss MA-6 UV Mask Aligner) at 390 nm wavelength for 29 s. The exposed wafer was then baked at 90 °C for 9 min and developed in SU-8 developer (PGMEA) for 2 min. The unexposed SU-8 was then rinsed off with IPA and DI water, and the wafer with the SU-8 channel mold was blow-dried with nitrogen gas. PDMS (poly(dimethylsiloxane)) was used to form the microchannel cavities from the SU-8 master mold. The closed microchannel is formed when the PDMS cavities are attached to the Si wafer. The Sylgard 184 silicone elastomer and its curing agent (Dow Corning) are mixed thoroughly at the mass ratio of 10:1 and baked at 70 °C for 3 h to accelerate the cross-linking reaction in the PDMS mixture and cure the PDMS slab. When the PDMS was cured, the PDMS slab was carefully detached from the master mold, and the inlet and outlet ports of the microchannel were formed by a puncher. The oxygen plasma treatment was applied to the microchannel to obtain a hydrophilic surface for the self-driven flow.

2.6. CA-125 Antigen Detection. The CA-125 antigen solution was prepared in PBS for the antigen detection experiments. The biosensors interacted with the CA-125 antigens in the antigen solution under both static and microfluidic shear flow conditions. In the static drop condition, 2 μL of CA-125 solution was dropped onto the biosensor statically. In the microfluidic flow condition, the biosensor was placed at a 5 mm location away from the microchannel inlet, and 2 μL of CA-125 solution was introduced into the inlet and encountered the biosensor in the microchannel. Figure S2 shows schematics of both conditions.

2.7. Electrical Measurement. *2.7.1. Capacitive Measurement.* The capacitance (C_p) measurements in all experiments of the biosensors were conducted with the electrical probe station (Signatone 8−250−5) connected to the LCR meter (GW Instek LCR8200). The capacitance readings in the experiments were measured within the frequency range from 10 kHz to 100 kHz with 10 kHz steps. The capacitance of the biosensor was measured for each step of the sensor layer fabrication and PBS without CA-125 antigen as the baseline reference signal. The capacitance signals for both PEG and AuNP-coated biosensors were measured for the following steps: (1) bare gold electrodes; (2) PEG-coated or AuNP-coated electrodes; (3) Ab immobilized biosensors; (4) PBS drop without CA-125 antigen on the biosensor (baseline signal for the Ag detection in static condition); (5) PBS flow without CA-125 antigen encounter biosensor in the microchannel (baseline signal for the Ag detection in microfluidic shear flow condition); (6) CA-125 antigen solution static drop on the sensor; (7) CA-125 antigen solution flow over biosensor in the microchannel. The capacitive signals were measured at 100 mV amplitude with 0.5 V voltage in all experiments.

2.7.2. Function of Interdigitated Capacitive Biosensor. Interdigitated electrodes have a higher surface area-to-volume ratio, which helps minimize the sensing system while providing more effective sensing areas compared to other capacitive biosensors.[53,54] IDEs can also be adapted for the detection of multiple antigens by adjusting their dimensions and spacings to match the scale of target antigens and antibodies. When a voltage is applied, IDEs generate electrical fields. The change in the dielectric properties of the medium between the IDEs and the coating layers on the IDEs can lead to variations in

https://doi.org/10.1021/acsomega.4c07596
ACS Omega 2025, 10, 692−702

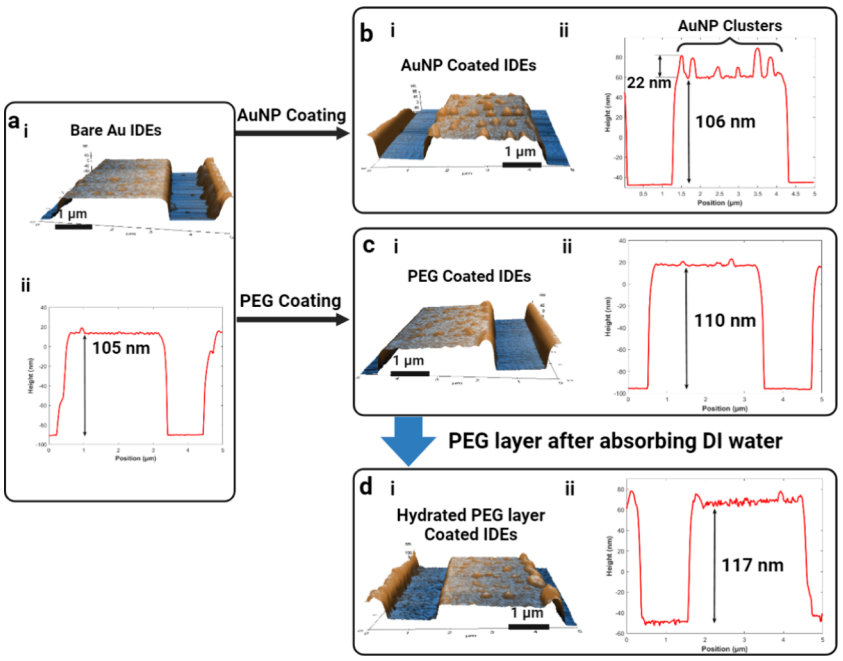

Figure 3. (a) (i) 3D AFM image of bare gold IDEs. (ii) Thickness scanning of bare gold IDEs. (b) (i) 3D AFM image of AuNP coated IDEs. (ii) Thickness scanning of AuNP-coated IDEs. (c) (i) 3D AFM image of PEG-coated IDEs. (ii) Thickness scanning of PEG-coated IDEs. (d) (i) 3D AFM image of DI water-hydrated PEG layer-coated IDEs. Thickness scanning of DI water-hydrated PEG layer-coated IDEs.

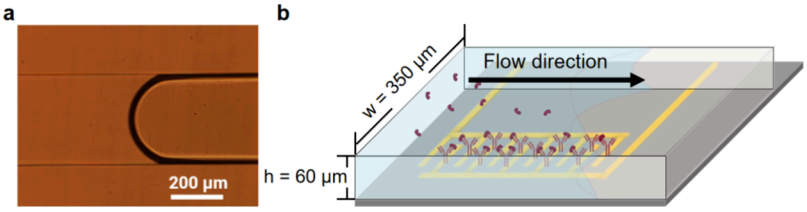

Figure 4. (a) Antigen solution flowing in the microchannel captured by the high-speed camera through the microscope. (b) Schematic diagram of microfluidic capillary shear flow on the biosensor in the microchannel.

capacitance measurements via an LCR meter. This mechanism allows for the detection of the CA-125 antigen through capacitance variations caused by changes in dielectric properties due to the conjugation of CA-125 antigens and antibodies. The electric capacitance measured by the IDEs can be expressed by eq 1.

$$C = \varepsilon_0 \varepsilon_r \frac{A_{eff}}{d_{eff}} \quad (1)$$

where C is the electric capacitance, ε_0 is the vacuum permittivity, ε_r is the relative permittivity of the medium on/between the electrodes, A_{eff} is the effective surface area of the IDEs, and d_{eff} is the effective distance between IDEs. Based on the homogeneous assumption of each layer coating on the IDEs, the electrical capacitance reading on the IDEs can be simulated by this equivalent model. More detailed explanation can be found in a previous study.[45]

3. RESULTS AND DISCUSSION

3.1. Surface Characterization of Functional Layers on Interdigitated Electrodes. In the fabrication of both PEG-coated and AuNP-coated biosensors, each layer played a critical role in antibody immobilization. For instance, a well-coated PEG layer insulated the IDEs, aligned the antibody immobilization directions, immobilized antibodies, and made the biosensor biocompatible and suitable for aqueous detection conditions. Similarly, the AuNP layer effectively immobilized antibodies, enhancing the sensitivity of the antigen detection. Atomic Force Microscopy (AFM) images were taken to confirm the presence of PEG and AuNP layers on the biosensor surface. Figure 3 shows the AFM images of bare IDEs, AuNP-coated IDEs, PEG-coated IDEs, and a PEG monolayer after absorbing water.

In Figure 3a, the AFM image displays a smooth surface of a 105 nm-thick gold electrode that was produced through e-beam deposition. Figure 3b shows the AFM image of the AuNP layer on the IDE. The humps in Figure 3b correspond to AuNP agglomerations on the IDE surface, with heights ranging from 22 to 30 nm, two to three times the diameter of individual AuNPs (~10 nm). Therefore, within an AuNP cluster, only a few nanoparticles directly bonded to the IDE surface, while the remainder were weakly agglomerated to those bonded to the surface. Hence, the agglomeration of AuNPs causes unstable antibody immobilization on the biosensor, leading to decreased reliability in its performance. The AFM image of the PEG-coated IDE, shown in Figure 3c, presents a smooth surface for the 110 nm-thick IDE, which was 5 nm thicker than the bare Au IDE due to the additional PEG coating. The smooth texture of the PEG-coated IDE suggests far fewer clusters on the surface, indicating the formation of a

https://doi.org/10.1021/acsomega.4c07596
ACS Omega 2025, 10, 692−702

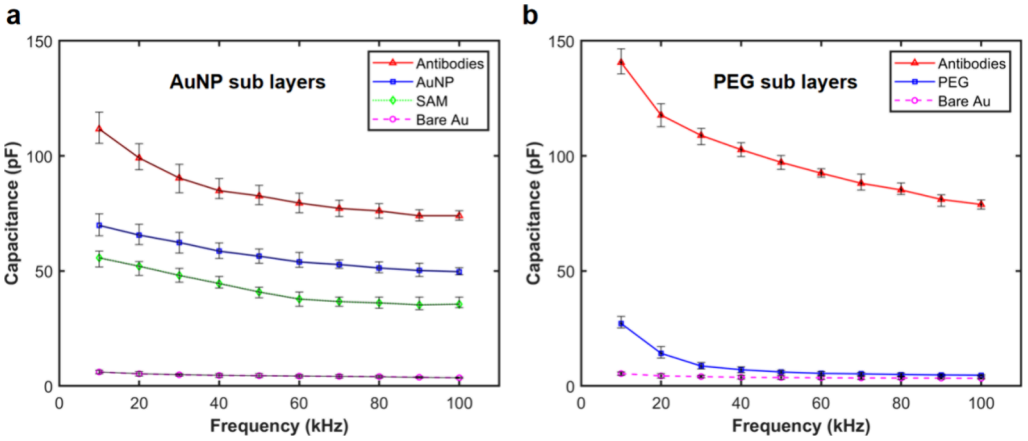

Figure 5. Capacitance measurement plot of (a) all sublayers of the AuNP-coated biosensor which are "bare IDEs", "SAM coating", "AuNP coating", and "antibodies immobilization" and (b) all sublayers of the PEG-coated biosensor which are "bare IDEs", "PEG coating", and "antibodies immobilization". Each data point is the average of three replicates.

PEG monolayer. This PEG monolayer ensured the presence of covalent bonds between antibodies and IDEs, enhancing the biosensor's potential under shear flow conditions.

To further confirm the PEG layer on the IDEs, Figure 3c,d presents comparative AFM scans of dry PEG-coated IDEs and PEG-coated IDEs after absorbing water. As PEG is a hygroscopic material that absorbs water and can expand significantly compared to its dry state,[52] the thickness of the PEG layer in the dry state measured approximately 5 nm and increased to 12 nm after water absorption-induced expansion. The consistent increase in thickness across the IDE surface further confirmed the uniform coating of the PEG layer on the IDE, indicating its readiness for antibody immobilization.

3.2. Shear Flow in Microfluidic Channel. A PDMS microchannel measuring 350 μm in width, 60 μm in depth, and 20 mm in length was used to create microfluidic shear flow conditions for the biosensors, as shown in Figure 4. Due to the inherent hydrophobic nature of PDMS, an oxygen plasma treatment was applied to the microchannel surface to induce a hydrophilic state and activate capillary action within the microchannel. The antigen solution flow was then driven by capillary action, generating shear stress on the biosensor surface. The shear stress at the biosensor surface is determined by the flow speed of the antigen solution relative to the channel height at the bottom surface. This shear stress can be determined using eq 2, which is based on the assumption of fully developed Poiseuille flow between infinite parallel plates, given the high aspect ratio of the microchannel.

$$\tau = \mu \frac{\partial U_x}{\partial y}\bigg|_{y=0} \approx \mu \frac{6Q}{wh^2} \tag{2}$$

where τ is the shear stress on the channel bottom surface, μ is the dynamic viscosity of the antigen solution which is 9.0×10^{-4} Pa·s, and U_x is the flow speed at the biosensor location (10 mm from channel inlet) measured using a high-speed camera (Phantom V-7.3) which is 22 mm/s. The flow rate of the antigen solution is calculated as 0.46 μL/s. "w" and "h" are the microchannel width and height, respectively. Therefore, the shear stress was calculated using eq $\tau = \mu \times 6Q/wh^2 = 1.92$ Pa, and it had an impact on the immobilization of CA-125 antibodies on the biosensor surface, consequently influencing the stability of CA-125 antigen detection using biosensors. A high shear force in flow can detach immobilized antibodies from unstable surfaces, such as agglomerated AuNPs, reducing binding efficiency and affecting specificity. Researchers have explored the use of tunable alternating current electrohydrodynamic (ac-EHD) forces to manipulate lateral fluid motion over electrodes, aiming to reduce nonspecific binding and enhance detection specificity.[55−58] However, for POC applications, a passive method to improve sensing is preferred, achieved through optimizing the biosensor's sensing interface. Flow control and sample preparation for optimizing assay kinetics are commonly employed in paper-based lateral flow assays (LFAs);[59−61] however, LFAs typically exhibit lower sensitivity, making it challenging to detect low concentrations of biomarkers in real samples, such as CA-125. In high-shear flow microfluidic systems with capacitive electrochemical biosensors, addressing the misalignment and detachment of immobilized probes caused by shear forces is critical for improving the availability of antigen-binding sites, thereby enhancing the sensitivity and repeatability of the detection process.

3.3. Electrical Measurement. *3.3.1. Capacitance Measurement of Each Functional Layer of PEG and AuNP-Based Biosensors.* PEG-coated and AuNP-coated biosensors were connected to an LCR meter through the probe station for capacitance measurements after each functional layer was formed during fabrication. The capacitive signal change measured for each sublayer helps confirm the formation of the functional layers. Figure 5 shows the plot of capacitance measurements for all sublayers, from bare IDEs to antibody-immobilized IDEs, of PEG-coated and AuNP-coated biosensors over frequencies ranging from 10 to 100 kHz in steps of 10 kHz.

From Figure 5a, the capacitance of the bare IDEs was first measured, decreasing from 6 pF at 10 kHz to 4 pF at 100 kHz. After coating with SAM, the capacitance increased to 56 pF at 10 kHz, mainly due to the formation of the SAM layer. The SAM coating on the IDEs provides insulation and induces changes in the capacitance measurements. The AuNP coating, having a higher permittivity, directly changed the dielectric properties on the IDE surface, resulting in an increase in capacitance measurement, recorded from 70 pF at 10 kHz to 50 pF at 100 kHz. Finally, the capacitance of the antibody-immobilized biosensor was measured at 112 pF at 10 kHz,

https://doi.org/10.1021/acsomega.4c07596
ACS Omega 2025, 10, 692−702

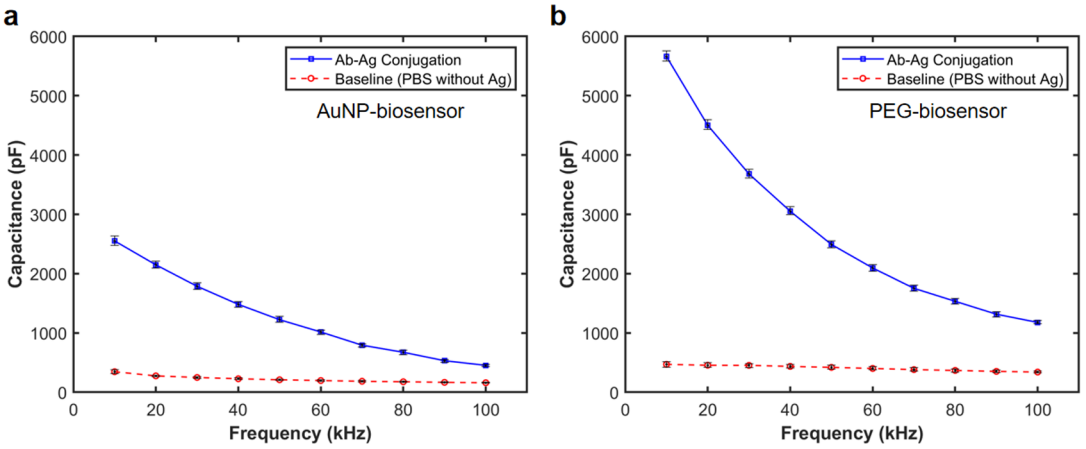

Figure 6. Capacitance measurements over the frequencies using the static drops of PBS with and without CA-125 antigens on different biosensors: (a) AuNP-coated biosensor and (b) PEG-coated biosensor. Each data point is the average of three replicates.

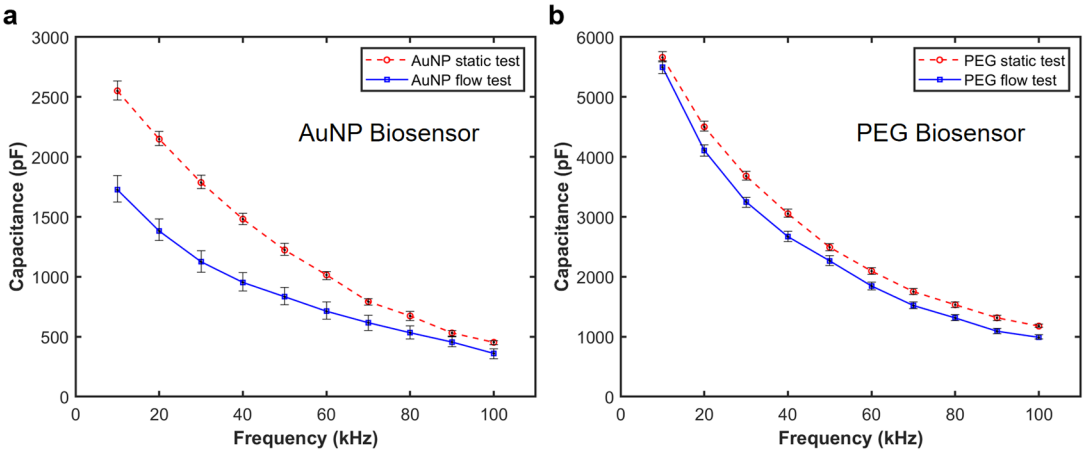

Figure 7. Capacitive measurement comparisons over frequency under static drop and microfluidic shear flow conditions for (a) AuNP-coated biosensor and (b) PEG-coated biosensor. Each data point is the average of three replicates.

reducing to 74 pF at 100 kHz. For all capacitance measurements, the capacitance decreases with increasing frequency due to the decrease in capacitive reactance.

In Figure 5b, due to the same fabrication process of the IDEs, the capacitive signals of bare IDEs are similar using the average values from six replicates in both plots. The capacitance measured on PEG-coated IDEs shows an increase due to the electrical insulation property of the PEG, confirming the PEG coating. As confirmed in Figure 3, the dry PEG monolayer is a thin layer about 5 nm thick, causing a notable change in the capacitive signal. The capacitance measured for the PEG monolayer was 27 pF at 10 kHz, decreasing to 5 pF at 100 kHz. After immobilizing the CA-125 antibodies onto the PEG monolayer, the capacitance measured on the biosensor increased to 141 pF at 10 kHz and decreased to 79 pF at 100 kHz.

3.3.2. Capacitance Measurement of CA-125 Antigen–Antibody Conjugation on the Biosensor. The CA-125 antigen detection experiments were conducted in two stages: (i) measuring the baseline capacitive signal using static PBS droplets without CA-125 antigen on the biosensors and (ii) measuring the capacitive signal of CA-125 antigen–antibody conjugation with a 500 U/ml antigen solution in PBS droplets on the biosensors. The results of these capacitance measurements are presented in Figure 6.

In Figure 6a, the capacitive signal of the PBS baseline for the AuNP-coated biosensor was measured at 346 pF at 10 kHz, decreasing to 160 pF at 100 kHz. In the PBS drop condition, PBS served as the dielectric medium between the IDEs, which has a much higher electrical permittivity than air, leading to a significant increase in capacitance. After applying a 500 nL drop of CA-125 antigen solution in PBS to the biosensor, the antigens reacted with the antibodies immobilized on the sensor surface, forming antigen–antibody complexes. These complexes altered the size and polarity of the molecules on the IDEs, which interfered with the original charges, contributing to the formation of a dipole moment.[62] This phenomenon enhanced polarization on the IDE surface and significantly increased the capacitance measured by the biosensor.[63] For the AuNP-coated biosensor, the capacitance measurements for antigen–antibody conjugation were recorded over frequencies from 10 to 100 kHz, with the highest value reaching 2551 pF at 10 kHz, a substantial increase from the baseline value of 346 pF at 10 kHz.

Figure 6b presents the capacitive signals measured using the same protocol as that with PEG-coated biosensors. The capacitance of the PBS baseline ranged from 470 to 340 pF over the same frequency range. PEG-2000, which is initially approximately 5 nm thick in its dry state, expands several times its original thickness in an aqueous environment due to its

https://doi.org/10.1021/acsomega.4c07596
ACS Omega 2025, 10, 692−702

hygroscopic properties,[54] leading to a thicker PEG monolayer. During this expansion, the PEG polymer chains absorbed polar water molecules, leading to a higher capacitance measurement for the PEG-coated biosensor's PBS baseline. The antigen−antibody conjugation detected by the PEG-coated biosensor showed a significantly higher capacitive measurement (5660 pF at 10 kHz) compared with the AuNP-coated biosensor (2551 pF at 10 kHz). The increased sensitivity with the PEG monolayer coating can be attributed to two main factors: (i) the hygroscopic property of PEG, which absorbs and stores water, thereby increasing polarity and amplifying the capacitive sensing signals, and (ii) the better alignment of antibody immobilization. Unlike the AuNP coating, where antibodies may bind randomly on the spherical particles, the brush-like structure of the PEG monolayer allows most antibodies to bind on the top surface, enhancing their interaction with antigens. Consequently, the PEG coating provides enhanced sensitivity for CA-125 antigen detection.

3.3.3. Capacitance Measurement Comparison of CA-125 Antigen−Antibody Conjugation in the Static Drop and Microfluidic Shear Flow Condition Using AuNP- and PEG-Coated biosensors. Understanding the biosensor performance under microfluidic shear flow is essential for integrating the biosensor into a microfluidic platform as a POC device. Therefore, the stability of AuNP- and PEG-coated biosensors under microfluidic shear flow was evaluated by comparing the capacitive measurements of CA-125 antigen−antibody conjugation in both static drop and microfluidic shear flow conditions, as shown in Figure 7.

The inherent tendency of AuNPs to agglomerate leads to clusters composed of two or more particles. As depicted in the AFM image, the AuNPs do not form a uniform monolayer, resulting in an uneven coating on the IDE surface due to agglomeration. This tendency is exacerbated during fabrication by the elevated ionic strength of PBS, which reduces the electrostatic repulsion and promotes clustering between AuNPs. During antibody immobilization, a significant portion of the antibodies, intended to bond to the AuNPs attached to the biosensor via peptide bonds, instead adhere to the AuNP clusters. These interactions within the AuNP clusters, driven by van der Waals and electrostatic forces, deviate from the designed peptide bonds between the AuNPs and the biosensors. As a result, the antibodies are prone to dissociating from the AuNP clusters under the shear flow conditions of microfluidics. This dissociation of AuNP-antibody complexes from the clusters leads to a substantial decrease in the capacitive signal of the AuNP-coated biosensor, dropping from 2551 pF in static drop conditions to 1726 pF under microfluidic shear flow, representing a 32.4% decrease in capacitance (ΔCp%↓), as illustrated in Figure 7a.

In contrast, PEG with a thiol group forms a stable monolayer on the gold surface of the IDEs,[64] preventing agglomeration effectively and allowing for uniform antibody immobilization through peptide bonds. This PEG monolayer is securely attached to the IDEs via covalent bonds, ensuring robust interactions. The robustness of these interactions is a key advantage as it ensures the stability and reliability of the biosensor. Additionally, the PEG monolayer provides a smoother surface, reducing friction during fluid flow and stabilizing the biosensing environment by absorbing water molecules from the aqueous environment. As a result, antibodies immobilized on the PEG monolayer remain securely attached under microfluidic shear flow, leading to only a minor change in the capacitive signal from 5660 pF in static drop conditions to 5498 pF under microfluidic shear flow, corresponding to a 2.9% decrease in capacitance (ΔCp %↓), as shown in Figure 7b.

4. CONCLUSIONS

This study examined the sensitivity of a capacitive biosensor utilizing PEG compared to AuNP as an immobilization nanomaterial. Surface characterizations through AFM analysis were conducted on both the AuNP and the PEG layers to understand their morphologies. The phenomenon of AuNP agglomeration led to antibodies bonding to the AuNPs on the surfaces of the clusters, making them susceptible to peeling off during microfluidic shear flow. In contrast, PEG offers several advantages in microfluidic applications, including a smooth monolayer coating, precise alignment for antibody immobilization, hydrophilic nature, and the ability to absorb water. These attributes collectively contribute to the stable detection of antigens using a PEG-coated biosensor under microfluidic shear flow conditions.

The results of our study demonstrate a significant enhancement in the sensitivity with the PEG-coated biosensor. The capacitive signal variation observed between CA-125 antigen−antibody conjugation and the PBS baseline was 1.6 times higher (at 10 kHz) with the PEG-coated biosensor compared to the signal variation of the AuNP-coated biosensor, indicating a clear advantage in sensitivity for the PEG-coated biosensor in detecting the CA-125 antigen.

Under microfluidic shear flow conditions, the capacitive signal typically measures lower than under static drop conditions due to the shear effect. For instance, a 32.4% decrease in the capacitive signal was observed with the AuNP-coated biosensor at 10 kHz under shear flow conditions. In contrast, the PEG-coated biosensor exhibited only a minor variation between microfluidic shear flow and static drop conditions with just a 2.9% reduction in the capacitive signal measured at 10 kHz. This suggests significantly improved stability of the PEG-coated biosensor in detecting CA-125 antigen under microfluidic shear flow compared with the AuNP-coated biosensor.

This study experimentally investigates the sensitivity and stability of CA-125 antigen detection using a PEG-coated biosensor under microfluidic shear flow conditions. In addition to its favorable performance in the microfluidic system, PEG's lower cost and ease of fabrication align well with the objectives of point-of-care diagnostic device applications. While PEG demonstrates enhanced sensitivity and stability for CA-125 antigen detection, its performance with other biomarkers in different types of biosensors under microfluidic conditions remains unexplored. Future efforts will focus on developing multiplex assays using PEG-coated biosensors for detecting multiple biomarkers on microfluidic platforms. Clinical studies with real patient samples will be essential to assessing the durability, sensitivity, and specificity of these biosensors. Additionally, a degradation study of PEG-coated biosensors will be crucial to ensure their reliability for POC applications.

■ ASSOCIATED CONTENT

Supporting Information

The Supporting Information is available free of charge at https://pubs.acs.org/doi/10.1021/acsomega.4c07596.

https://doi.org/10.1021/acsomega.4c07596
ACS Omega 2025, 10, 692−702

(Figure S1) Interdigitated electrodes (IDEs) fabrication process using E-beam lithography and physical vapor deposition techniques; (Figure S2) schematics of the CA-125 antigen detection experimental setups: CA-125 antigen detection in static drop condition and microfluidic shear flow condition; (Figure S3) schematic diagrams of different layers of PEG-coated biosensor structure and different layers of AuNP-coated biosensor structure (PDF)

AUTHOR INFORMATION

Corresponding Author

Eon Soo Lee − *Advanced Energy Systems and Microdevices Laboratory, Department of Mechanical and Industrial Engineering, New Jersey Institute of Technology, Newark, New Jersey 07102, United States;* orcid.org/0000-0001-5863-3108; Phone: +1 973 596 3318; Email: eonsoo.lee@njit.edu

Authors

Yudong Wang − *Advanced Energy Systems and Microdevices Laboratory, Department of Mechanical and Industrial Engineering, New Jersey Institute of Technology, Newark, New Jersey 07102, United States*

Niladri Talukder − *Advanced Energy Systems and Microdevices Laboratory, Department of Mechanical and Industrial Engineering, New Jersey Institute of Technology, Newark, New Jersey 07102, United States;* orcid.org/0000-0003-0332-8055

Bharath Babu Nunna − *Department of Mechanical Engineering, Weber State University, Ogden, Utah 84408, United States; Division of Engineering in Medicine, Department of Medicine, Brigham and Women's Hospital, Harvard Medical School, Harvard University, Cambridge, Massachusetts 02139, United States; Harvard Graduate School of Education, Harvard University, Cambridge, Massachusetts 02138, United States*

Ming Lu − *The Center for Functional Nanomaterials, Brookhaven National Laboratory, Upton, New York 11973, United States*

Xiao Tong − *The Center for Functional Nanomaterials, Brookhaven National Laboratory, Upton, New York 11973, United States*

Complete contact information is available at: https://pubs.acs.org/10.1021/acsomega.4c07596

Notes

The authors declare no competing financial interest.

ACKNOWLEDGMENTS

The authors acknowledge the research support from the New Jersey Institute of Technology (NJIT) and the National Science Foundation (grant ID: NSF 2318433). This research used Nanofabrication facility and Proximal Probes facility of the Center for Functional Nanomaterials (CFN), which is a U.S. Department of Energy Office of Science User Facility, at Brookhaven National Laboratory under contract no. DE-SC0012704.

REFERENCES

(1) Mattiasson, B.; Teeparuksapun, K.; Hedström, M. Immunochemical Binding Assays for Detection and Quantification of Trace Impurities in Biotechnological Production. *Trends Biotechnol.* **2010**, *28* (1), 20−27.

(2) Borisov, S. M.; Wolfbeis, O. S. Optical Biosensors. *Chem. Rev.* **2008**, *108* (2), 423−461.

(3) Ronkainen, N. J.; Halsall, H. B.; Heineman, W. R. Electrochemical Biosensors. *Chem. Soc. Rev.* **2010**, *39* (5), 1747−1763.

(4) Pohanka, M. The Piezoelectric Biosensors: Principles and Applications. *Int. J. Electrochem. Sci.* **2017**, *12*, 496−506.

(5) Ramanathan, K.; Danielsson, B. Principles and Applications of Thermal Biosensors. *Biosens. Bioelectron.* **2001**, *16* (6), 417−423.

(6) da Silva, E. T. S. G.; Souto, D. E. P.; Barragan, J. T. C.; de F. Giarola, J.; de Moraes, A. C. M.; Kubota, L. T. Electrochemical Biosensors in Point-of-Care Devices: Recent Advances and Future Trends. *ChemElectroChem.* **2017**, *4* (4), 778−794.

(7) Yoon, J. Y. Introduction to biosensors: From electric circuits to immunosensors. In *Introduction to Biosensors*; Springer: 2016.

(8) Berggren, C.; Bjarnason, B.; Johansson, G. Capacitive Biosensors. *Electroanalysis* **2001**, *13* (3), 173−180.

(9) Ertürk, G.; Mattiasson, B. Capacitive Biosensors and Molecularly Imprinted Electrodes. *Sensors* **2017**, *17* (2), 390.

(10) Bange, A.; Halsall, H. B.; Heineman, W. R. Microfluidic Immunosensor Systems. *Biosens. Bioelectron.* **2005**, *20* (12), 2488−2503.

(11) Wang, Y.; Nunna, B. B.; Talukder, N.; Etienne, E. E.; Lee, E. S. Blood Plasma Self-Separation Technologies During the Self-Driven Flow in Microfluidic Platforms. *Bioengineering* **2021**, *8* (7), 94.

(12) Etienne, E. E.; Nunna, B. B.; Talukder, N.; Wang, Y.; Lee, E. S. COVID-19 Biomarkers and Advanced Sensing Technologies for Point-of-Care (POC) Diagnosis. *Bioengineering* **2021**, *8* (7), 98.

(13) Nunna, B. B.; Mandal, D.; Lee, J. U.; Zhuang, S.; Lee, E. S. Sensitivity Study of Cancer Antigens (CA-125) Detection Using Interdigitated Electrodes Under Microfluidic Flow Condition. *BioNanoScience* **2019**, *9*, 203−214.

(14) Nunna, B. B.; Mandal, D.; Zhuang, S.; Lee, E. S. A Standalone Micro Biochip to Monitor the Cancer Progression by Measuring Cancer Antigens as a Point-of-Care (POC) Device for Enhanced Cancer Management. In *2017 IEEE Healthcare Innovations and Point of Care Technologies (HI-POCT)*; IEEE, *2017*; pp 212−215.

(15) Nunna, B. B.; Mandal, D.; Zhuang, S.; Lee, E. S. Innovative Point-of-Care (POC) Micro Biochip for Early Stage Ovarian Cancer Diagnostics. *Sens. Transducers* **2017**, *214* (7), 12.

(16) Nunna, B. B.; Zhuang, S.; Javier, J.; Mandal, D.; Lee, E. S. Biomolecular Detection Using Molecularly Imprinted Polymers (MIPs) at Point-of-Care (POC) Micro Biochip. In *Proceedings of the 2016 IEEE-NIH 2016 Healthcare Innovation Point of Care Technologies Conference HI POCT16, PCHT16−0099*; IEEE: Cancun, Mexico, 2016; pp 9−11.

(17) Wang, Y.; Talukder, N.; Nunna, B. B.; Lee, E. S. Dean Vortex-Enhanced Blood Plasma Separation in Self-Driven Spiral Microchannel Flow with Cross-Flow Microfilters. *Biomicrofluidics* **2024**, *18* (1). DOI: .

(18) Choi, S.; Goryll, M.; Sin, L. Y. M.; Wong, P. K.; Chae, J. Microfluidic-Based Biosensors Toward Point-of-Care Detection of Nucleic Acids and Proteins. *Microfluid. Nanofluid.* **2011**, *10*, 231−247.

(19) Reinholt, S. J.; Craighead, H. G. Microfluidic Device for Aptamer-Based Cancer Cell Capture and Genetic Mutation Detection. *Anal. Chem.* **2018**, *90* (4), 2601−2608.

(20) Zhou, Q.; Rahimian, A.; Son, K.; Shin, D. S.; Patel, T.; Revzin, A. Development of an Aptasensor for Electrochemical Detection of Exosomes. *Methods* **2016**, *97*, 88−93.

(21) Xu, H.; Liao, C.; Zuo, P.; Liu, Z.; Ye, B. C. Magnetic-Based Microfluidic Device for On-Chip Isolation and Detection of Tumor-Derived Exosomes. *Anal. Chem.* **2018**, *90* (22), 13451−13458.

(22) Huang, C. H.; Lee, K. C.; Doudna, J. A. Applications of CRISPR-Cas Enzymes in Cancer Therapeutics and Detection. *Trends Cancer* **2018**, *4* (7), 499−512.

(23) Nunna, B. B.; Wang, Y.; Talukder, N.; Lee, E. S. Capillary Flow Dynamics of Blood with Varied Hematocrit in Microfluidic Platforms.

In *2022 IEEE Healthcare Innovations and Point of Care Technologies (HI-POCT)*; IEEE, 2022; pp 1−4.
(24) Felder, M.; Kapur, A.; Gonzalez-Bosquet, J.; Horibata, S.; Heintz, J.; Albrecht, R.; Fass, L.; Kaur, J.; Hu, K.; Shojaei, H.; Whelan, R. J.; Patankar, M. S. MUC16 (CA125): Tumor Biomarker to Cancer Therapy, a Work in Progress. *Mol. Cancer* **2014**, *13* (1), 1−15.
(25) Olson, S. H.; Mignone, L.; Nakraseive, C.; Caputo, T. A.; Barakat, R. R.; Harlap, S. Symptoms of Ovarian Cancer. *Obstet. Gynecol.* **2001**, *98* (2), 212−217.
(26) Torre, L. A.; Trabert, B.; DeSantis, C. E.; Miller, K. D.; Samimi, G.; Runowicz, C. D.; Gaudet, M. M.; Jemal, A.; Siegel, R. L. Ovarian Cancer Statistics, 2018. *CA Cancer J. Clin.* **2018**, *68* (4), 284−296.
(27) Weiland, F.; Fritz, K.; Oehler, M. K.; Hoffmann, P. Methods for Identification of CA125 from Ovarian Cancer Ascites by High Resolution Mass Spectrometry. *Int. J. Mol. Sci.* **2012**, *13* (8), 9942−9958.
(28) Jin, H.; Gui, R.; Gong, J.; Huang, W. Aptamer and 5-Fluorouracil Dual-Loading Ag_2S Quantum Dots Used as a Sensitive Label-Free Probe for Near-Infrared Photoluminescence Turn-On Detection of CA125 Antigen. *Biosens. Bioelectron.* **2017**, *92*, 378−384.
(29) Hamd-Ghadareh, S.; Salimi, A.; Fathi, F.; Bahrami, S. An Amplified Comparative Fluorescence Resonance Energy Transfer Immunosensing of CA125 Tumor Marker and Ovarian Cancer Cells Using Green and Economic Carbon Dots for Bio-Applications in Labeling, Imaging, and Sensing. *Biosens. Bioelectron.* **2017**, *96*, 308−316.
(30) Suwansa-ard, S.; Kanatharana, P.; Asawatreratanakul, P.; Wongkittisuksa, B.; Limsakul, C.; Thavarungkul, P. Comparison of Surface Plasmon Resonance and Capacitive Immunosensors for Cancer Antigen 125 Detection in Human Serum Samples. *Biosens. Bioelectron.* **2009**, *24* (12), 3436−3441.
(31) Zhang, K.; Shen, X. Cancer Antigen 125 Detection Using the Plasmon Resonance Scattering Properties of Gold Nanorods. *Analyst* **2013**, *138* (6), 1828−1834.
(32) Al-Ogaidi, I.; Gou, H.; Aguilar, Z. P.; Guo, S.; Melconian, A. K.; Al-Kazaz, A. K. A.; Meng, F.; Wu, N. Detection of the Ovarian Cancer Biomarker CA-125 Using Chemiluminescence Resonance Energy Transfer to Graphene Quantum Dots. *Chem. Commun.* **2014**, *50* (11), 1344−1346.
(33) Prodromidis, M. I. Impedimetric Immunosensors—A Review. *Electrochim. Acta* **2010**, *55* (14), 4227−4233.
(34) Daniels, J. S.; Pourmand, N. Label-Free Impedance Biosensors: Opportunities and Challenges. *Electroanalysis* **2007**, *19* (12), 1239−1257.
(35) Mandal, D.; Nunna, B. B.; Zhuang, S.; Rakshit, S.; Lee, E. S. Carbon Nanotubes Based Biosensor for Detection of Cancer Antigens (CA-125) Under Shear Flow Condition. *Nano-Struct. Nano-Obj.* **2018**, *15*, 180−185.
(36) Wang, J.; Yau, S. T. Field-Effect Amperometric Immuno-Detection of Protein Biomarker. *Biosens. Bioelectron.* **2011**, *29* (1), 210−214.
(37) Wu, L.; Yan, F.; Ju, H. An Amperometric Immunosensor for Separation-Free Immunoassay of CA125 Based on Its Covalent Immobilization Coupled with Thionine on Carbon Nanofiber. *J. Immunol. Methods* **2007**, *322* (1−2), 12−19.
(38) Torati, S. R.; Kasturi, K. C.; Lim, B.; Kim, C. Hierarchical Gold Nanostructures Modified Electrode for Electrochemical Detection of Cancer Antigen CA125. *Sens. Actuators, B* **2017**, *243*, 64−71.
(39) Gasparotto, G.; Costa, J. P. C.; Costa, P. I.; Zaghete, M. A.; Mazon, T. Electrochemical Immunosensor Based on ZnO Nanorods−Au Nanoparticles Nanohybrids for Ovarian Cancer Antigen CA-125 Detection. *Mater. Sci. Eng., C* **2017**, *76*, 1240−1247.
(40) Ravalli, A.; Dos Santos, G. P.; Ferroni, M.; Faglia, G.; Yamanaka, H.; Marrazza, G. New Label-Free CA125 Detection Based on Gold Nanostructured Screen-Printed Electrode. *Sens. Actuators, B* **2013**, *179*, 194−200.
(41) Samadi Pakchin, P.; Ghanbari, H.; Saber, R.; Omidi, Y. Electrochemical Immunosensor Based on Chitosan-Gold Nanoparticle/Carbon Nanotube as a Platform and Lactate Oxidase as a Label for Detection of CA125 Oncomarker. *Biosens. Bioelectron.* **2018**, *122*, 68−74.
(42) Taleat, Z.; Ravalli, A.; Mazloum-Ardakani, M.; Marrazza, G. CA 125 Immunosensor Based on Poly-Anthranilic Acid Modified Screen-Printed Electrodes. *Electroanalysis* **2013**, *25* (1), 269−277.
(43) Wu, L.; Chen, J.; Du, D.; Ju, H. Electrochemical Immunoassay for CA125 Based on Cellulose Acetate Stabilized Antigen/Colloidal Gold Nanoparticles Membrane. *Electrochim. Acta* **2006**, *51* (7), 1208−1214.
(44) Wang, X.; Deng, W.; Shen, L.; Yan, M.; Yu, J. A 3D Electrochemical Immunodevice Based on an Au Paper Electrode and Using Au Nanoflowers for Amplification. *New J. Chem.* **2016**, *40* (3), 2835−2842.
(45) Nunna, B. B.; Mandal, D.; Lee, J. U.; Singh, H.; Zhuang, S.; Misra, D.; Bhuyian, M. N. U.; Lee, E. S. Detection of Cancer Antigens (CA-125) Using Gold Nanoparticles on Interdigitated Electrode-Based Microfluidic Biosensor. *Nano Convergence* **2019**, *6*, 1−12.
(46) Zheng, Y.; Wang, H.; Ma, Z. A Nanocomposite Containing Prussian Blue, Platinum Nanoparticles, and Polyaniline for Multi-Amplification of the Signal of Voltammetric Immunosensors: Highly Sensitive Detection of Carcinoma Antigen 125. *Microchim. Acta* **2017**, *184*, 4269−4277.
(47) Goddard, J. M.; Erickson, D. Bioconjugation Techniques for Microfluidic Biosensors. *Anal. Bioanal. Chem.* **2009**, *394*, 469−479.
(48) Shrewsbury, P. J.; Muller, S. J.; Liepmann, D. Effect of Flow on Complex Biological Macromolecules in Microfluidic Devices. *Biomed. Microdevices* **2001**, *3*, 225−238.
(49) Simone, G.; Perozziello, G.; Battista, E.; De Angelis, F.; Candeloro, P.; Gentile, F.; Malara, N.; Manz, A.; Carbone, E.; Netti, P.; Di Fabrizio, E. Cell Rolling and Adhesion on Surfaces in Shear Flow. A Model for an Antibody-Based Microfluidic Screening System. *Microelectron. Eng.* **2012**, *98*, 668−671.
(50) Christensen, M.; Frosch, M.; Jensen, P.; Schnell, U.; Shashoua, Y.; Nielsen, O. F. Waterlogged Archaeological Wood—Chemical Changes by Conservation and Degradation. *J. Raman Spectrosc.* **2006**, *37* (10), 1171−1178.
(51) Truong, V.; Blakey, I.; Whittaker, A. K. Hydrophilic and Amphiphilic Polyethylene Glycol-Based Hydrogels with Tunable Degradability Prepared by "Click" Chemistry. *Biomacromolecules* **2012**, *13* (12), 4012−4021.
(52) Mehne, J.; Markovic, G.; Pröll, F.; Schweizer, N.; Zorn, S.; Schreiber, F.; Gauglitz, G. Characterisation of Morphology of Self-Assembled PEG Monolayers: A Comparison of Mixed and Pure Coatings Optimised for Biosensor Applications. *Anal. Bioanal. Chem.* **2008**, *391*, 1783−1791.
(53) Zou, Z.; Kai, J.; Rust, M. J.; Han, J.; Ahn, C. H. Functionalized Nano Interdigitated Electrodes Arrays on Polymer with Integrated Microfluidics for Direct Bio-Affinity Sensing Using Impedimetric Measurement. *Sens. Actuators, A* **2007**, *136* (2), 518−526.
(54) Tan, S. H.; Nguyen, N. T.; Chua, Y. C.; Kang, T. G. Oxygen Plasma Treatment for Reducing Hydrophobicity of a Sealed Polydimethylsiloxane Microchannel. *Biomicrofluidics* **2010**, *4* (3), No. 032204.
(55) Shiddiky, M. J.; Vaidyanathan, R.; Rauf, S.; Tay, Z.; Trau, M. Molecular Nanoshearing: An Innovative Approach to Shear Off Molecules with AC-Induced Nanoscopic Fluid Flow. *Sci. Rep.* **2014**, *4* (1), 3716.
(56) Vaidyanathan, R.; Shiddiky, M. J. A.; Rauf, S.; Dray, E.; Tay, Z.; Trau, M. Tunable "Nano-Shearing": A Physical Mechanism to Displace Nonspecific Cell Adhesion During Rare Cell Detection. *Anal. Chem.* **2014**, *86* (4), 2042−2049.
(57) Grewal, Y. S.; Shiddiky, M. J.; Spadafora, L. J.; Cangelosi, G. A.; Trau, M. Nano-yeast−scFv probes on screen-printed gold electrodes for detection of *Entamoeba histolytica* antigens in a biological matrix. *Biosens. Bioelectron.* **2014**, *55*, 417−422.
(58) Vaidyanathan, R.; Rauf, S.; Dray, E.; Shiddiky, M. J. A.; Trau, M. Alternating Current Electrohydrodynamics Induced Nanoshearing and Fluid Micromixing for Specific Capture of Cancer Cells. *Chem. - Eur. J.* **2014**, *20* (13), 3724−3729.

https://doi.org/10.1021/acsomega.4c07596
ACS Omega 2025, 10, 692−702

(59) Tang, R.; Yang, H.; Gong, Y.; Liu, Z.; Li, X.; Wen, T.; Qu, Z.; Zhang, S.; Mei, Q.; Xu, F. Improved Analytical Sensitivity of Lateral Flow Assay Using Sponge for HBV Nucleic Acid Detection. *Sci. Rep.* **2017**, *7* (1), 1360.
(60) Rivas, L.; Medina-Sánchez, M.; De La Escosura-Muñiz, A.; Merkoçi, A. Improving Sensitivity of Gold Nanoparticle-Based Lateral Flow Assays by Using Wax-Printed Pillars as Delay Barriers of Microfluidics. *Lab Chip* **2014**, *14* (22), 4406−4414.
(61) Jiang, X.; Fan, Z. H. Fabrication and Operation of Paper-Based Analytical Devices. *Annu. Rev. Anal. Chem.* **2016**, *9* (1), 203−222.
(62) Limbut, W.; Kanatharana, P.; Mattiasson, B.; Asawatreratanakul, P.; Thavarungkul, P. A Reusable Capacitive Immunosensor for Carcinoembryonic Antigen (CEA) Detection Using Thiourea Modified Gold Electrode. *Anal. Chim. Acta* **2006**, *561* (1−2), 55−61.
(63) Kallempudi, S. S.; Gurbuz, Y. A Nanostructured-Nickel Based Interdigitated Capacitive Transducer for Biosensor Applications. *Sens. Actuators, B* **2011**, *160* (1), 891−898.
(64) Cerruti, M.; Fissolo, S.; Carraro, C.; Ricciardi, C.; Majumdar, A.; Maboudian, R. Poly(Ethylene Glycol) Monolayer Formation and Stability on Gold and Silicon Nitride Substrates. *Langmuir* **2008**, *24* (19), 10646−10653.

https://doi.org/10.1021/acsomega.4c07596
ACS Omega 2025, 10, 692−702